


Article

Covalent Organic Frameworks for Simultaneous CO₂ Capture and Selective Catalytic Transformation

Yaling Li¹, Jianqiang Zhang¹, Kaiming Zuo¹, Zhongping Li², Yu Wang³, Hui Hu¹, Chaoyuan Zeng^{1,*}, Huanjun Xu¹, Baoshan Wang^{4,*} and Yanan Gao^{1,*} 

¹ Key Laboratory of Ministry of Education for Advanced Materials in Tropical Island Resources, Hainan University, No 58, Renmin Avenue, Haikou 570228, China; liyaling@hainanu.edu.cn (Y.L.); zhangjianq1995@sina.com (J.Z.); zuokaiming@hainanu.edu.cn (K.Z.); hhu@hainanu.edu.cn (H.H.); xhj1986@hainanu.edu.cn (H.X.)

² Department of Chemistry, Faculty of Science, National University of Singapore, 3 Science Drive 3, Singapore 117543, Singapore; lizhongping2013@163.com

³ School of Light Industry and Chemical Engineering, Dalian Polytechnic University, 1 Qinggongyuan, Dalian 116034, China; wang_yu@dlpu.edu.cn

⁴ Key Laboratory of Biomedical Polymers (Ministry of Education), College of Chemistry and Molecular Sciences, Wuhan University, Wuhan 430072, China

* Correspondence: zengchaoyuan@hainanu.edu.cn (C.Z.); baoshan@whu.edu.cn (B.W.); ygao@hainanu.edu.cn (Y.G.)

Abstract: Combination of capture and simultaneous conversion of CO₂ into valuable chemicals is a fascinating strategy for reducing CO₂ emissions. Therefore, searching for heterogeneous catalysts for efficient catalytic conversion of CO₂ is of great importance for carbon capture and utilization. Herein, we report a metalloporphyrin-based covalent organic framework (Co(II)@TA-TF COF) that can capture CO₂ and simultaneously convert it into cyclic carbonates under mild conditions. The COF was designed to possess micropores for the adsorption of CO₂ and integrated with cobalt(II) porphyrin (Co(II)@TAPP) units as catalytic sites into the vertices of the layered tetragonal networks. The structure of the Co(II)@TA-TF COF is unique where Co(II)@TAPP units are alternately stacked along the z direction with a slipped distance of 1.7 Å, which gives an accessible space to accommodate small molecules, making it possible to expose catalytic sites to substrates within the adjacent stacked layers. As a result, this COF is found to be highly effective for the addition of CO₂ and epoxides. Importantly, the Co(II)@TA-TF COF exhibited a dramatic size selectivity for substrates. In conjunction with its reusability, our results highlight the development of a new function of COFs for targeting simultaneous CO₂ absorption and utilization upon complementary exploration of the structural features of skeletons and pores. Such promising catalytic performance of the COF makes it possible for its potential practical application.

Keywords: covalent organic framework; carbon dioxide capture; cyclic carbonate; heterogeneous catalysts; carbon dioxide conversion; size-selectivity; carbon resource



Citation: Li, Y.; Zhang, J.; Zuo, K.; Li, Z.; Wang, Y.; Hu, H.; Zeng, C.; Xu, H.; Wang, B.; Gao, Y. Covalent Organic Frameworks for Simultaneous CO₂ Capture and Selective Catalytic Transformation. *Catalysts* **2021**, *11*, 1133. <https://doi.org/10.3390/catal11091133>

Academic Editor: Jin-Hyo Boo

Received: 4 July 2021

Accepted: 14 September 2021

Published: 21 September 2021

Publisher's Note: MDPI stays neutral with regard to jurisdictional claims in published maps and institutional affiliations.



Copyright: © 2021 by the authors. Licensee MDPI, Basel, Switzerland. This article is an open access article distributed under the terms and conditions of the Creative Commons Attribution (CC BY) license (<https://creativecommons.org/licenses/by/4.0/>).

1. Introduction

In the past few decades, the wanton emission of greenhouse gases has caused many serious environmental issues such as global warming, climate change, etc. Among all the greenhouse gases, carbon dioxide (CO₂) is recognized as the major anthropogenic greenhouse gas. Therefore, CO₂ capture has attracted much interest in the scientific community in order to reduce the implications for global warming. Meanwhile, CO₂ is the most abundant and renewable carbon resource on the earth. It is expected that effective capture and simultaneous conversion of CO₂ into valuable chemicals would definitely contribute to the development of the low-carbon economy [1,2]. As an attractive C₁ building block in organic synthesis, CO₂ has been converted into a variety of useable chemicals [3,4]. One of the most attractive products in this area is cyclic carbonates, which have been

synthesized from CO₂ and epoxides with high atom efficiency and have been widely used as raw materials for the production of polycarbonates, as aprotic polar solvents, and as pharmaceutical/fine chemical intermediates [5,6].

To date, a plethora of catalysts have been developed for this transformation. In earlier research, homogeneous organocatalysts, such as Schiff bases and organic bases [7], organic salts [8,9], metal Salen complexes [10,11] and metalloporphyrin complexes [12,13] have been used as effective catalysts for this reaction. However, difficult recycle of homogeneous catalysts limits their practical application. To this end, a variety of heterogeneous catalysts have been developed in the last ten years [14–19]. For instance, Ahmed and Sakthivel synthesized a series of amine functionalized silicoaluminophosphate (SAPO-34) materials that exhibited promising catalytic capability with high epichlorohydrin conversion (>80%) and selectivity to cyclic carbonate (>94%) [20]. Bhin et al. [21] prepared ZIF-95 and evaluated its catalytic performance in the addition of CO₂ to epoxides. Their research demonstrated that 83.2% conversion for propylene oxide (PO) was achieved with a selectivity of >99%. Methylated nitrogen-substituted silica SBA-15 [22], and amine incorporating organosilica nanotubes [23] were also found to be promising catalysts for the cycloaddition of CO₂ and epoxides. Moreover, a highly cross-linked microporous polymer matrix with grafted ionic liquid was developed as promising catalyst for the reaction by Han group [24]. Various CO₂-attracting groups and catalytically active sites were later incorporated onto the polymers to facilitate CO₂ adsorption and thus catalytic transformation [25–28]. Moreover, metal oxides were also attempted for the cyclic carbonate synthesis. For example, tetraoxo-coordinated zinc oxides were found to be highly active and the TOF can even reach up to 22,000 h⁻¹ for the reaction of 1,2-epoxyhexane with CO₂ at 120 °C and 3 MPa pressure [29]. In addition, metal organic frameworks (MOFs) have been shown to be highly active for cyclic carbonate synthesis. High porosity and unsaturated metal sites of MOFs make them ideal candidates for epoxide activation. However, poor availability and accessibility of active sites of MOFs limit their applications [30].

Although great progress and development have been made in heterogeneous catalysts, most of them are active only at high temperatures and high pressures. The development of an efficient heterogeneous catalyst for synthesizing cyclic carbonates under mild reaction conditions is of immense significance nowadays [31,32]. Thus, there is considerable interest to design and synthesize a material that is capable of capturing and simultaneously converting CO₂ into cyclic carbonates under mild conditions.

Covalent organic frameworks (COFs), a class of porous crystalline materials that allow the atomically precise integration of building units into porous structure, have gained much attention in gas storage and separation [33–40], heterogeneous catalysis [41–50], and optoelectronics [51,52]. COFs are entirely composed of light elements that are linked by strong covalent bonds to make highly porous materials with predictable structures [53–55]. With these features, COFs possess not only extremely high surface areas but also extraordinarily low densities, thus rendering them promising candidates for CO₂ adsorption materials [56–58]. Moreover, their properties can be tailored to fulfill a specific purpose through the choice of appropriate building units or pore surface functionalization. As such, COFs have been employed as catalysts or catalyst supports for the cyclic carbonate synthesis [59,60]. Using a bottom-up synthesis strategy, two-dimensional (2D) COF (OMe-OH-TPBP-COF) with both hydroxyl and methoxyl groups were designed by Chen group and exhibited good catalytic activity and efficiency for CO₂ cycloaddition (91% yield) under mild conditions (40 °C, 0.1 MPa CO₂) [59]. A triazine-linked COF (COF-JLU7) was also found to be a highly effective catalyst to convert CO₂ into cyclic carbonates under mild conditions [60]. Zhang et al. introduced ionic moiety into a metalloporphyrin-based COF through a post-synthesis strategy [61]. Although a high yield of propylene carbonate (>97%) was achieved, a high-temperature and high-pressure condition (120 °C, 2.5 MPa CO₂) was required. Similarly, a zinc-porphyrin COF (COF-366-Zn) also gave good cyclic carbonates yield, but the reaction needs acetonitrile as solvent and the reaction condition is still harsh (120 °C, 1.5 MPa CO₂) [62]. Due to pre-designability and easy-modification,

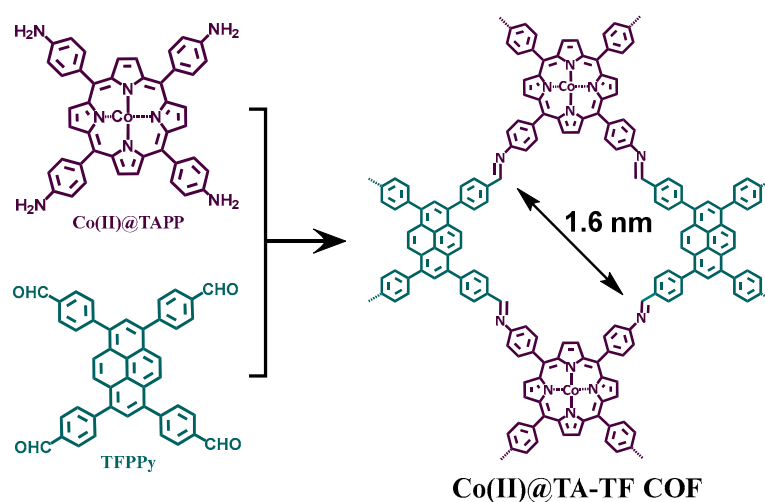
COFs have been used as catalyst supports for cyclic carbonate synthesis, ionic liquid [63,64] or poly (ionic liquid)s [65], copper oxide nanoparticles [66] and ionic polymer [67] were grafted within the frameworks of COFs that provided promising catalytic performance. However, it is difficult to realize substrate size for such catalytic systems as reactions proceed through one-dimensional (1D) channels of COFs. Therefore, searching for a catalyst with high selectivity of target products remains a challenge.

Herein, we fabricate a cobalt-porphyrin COF, termed Co(II)@TA-TF COF, that was constructed based on positive-charged cobalt-porphyrin building block and negative-charged pyrene building block. Electrostatic attraction of two different type building blocks leads to their alternately stacked arrangement, which affords an accessible space to accommodate small-molecular substrates for CO₂ cycloaddition reaction. High porosity and Lewis acidity of cobalt-porphyrin in this material allows for strong CO₂ adsorption and high efficiency in catalysis reaction. More importantly, the unique structure of the COF also leads to high substrate-size-selective performance towards cycloaddition reactions.

2. Results and Discussion

2.1. Synthesis and Characterization of the COF

In this work, Co(II)@TA-TF COF was synthesized by solvothermal reaction of cobalt(II) 5,10,15,20-tetrakis(4-aminophenyl)porphyrin (Co(II)@TAPP) and 1,3,6,8-tetrakis(4-formyl phenyl)pyrene (TFPPy) (Scheme 1) in a mixture of 1,4-dioxane/mesitylene/*N,N*-dimethyl acetamide (7:7:5 by volume) in the presence of 3 M acetic acid, followed by heating at 140 °C for 3 days, which afforded a brownish solid in 85% yield (see details in the supporting information, SI, Section S1). Although both building units bear four linker groups, which is disadvantageous to the “error checking” and “proof-reading” processes for the formation of COFs in principle, a crystalline Co(II)@TA-TF COF solid has still been obtained. Elemental analysis confirmed that the C, H and N contents of the Co(II)@TA-TF COF were close to the theoretical values (Table S1). Fourier-transform infrared (FT-IR) spectra showed a C=N stretching vibration band at 1620 cm⁻¹, indicative of the formation of imine linkages (Figure S1).



Scheme 1. Synthesis of the Co(II)@TA-TF COF.

The crystalline structure of the Co(II)@TA-TF COF was revealed by powder X-ray diffraction (PXRD) in combination with structural simulations (Figure 1). In a general way, a most possible eclipsed AA stacking structure (space group: *Pmmm*) was firstly simulated, where Co(II)@TAPP units were stacked vertically with adjacent Co(II)@TAPP units along *z* direction, and so do TFPPy units (Figure S2). We denominate this stacking as TA-TA + TF-TF AA structure. Based on this arrangement, a horizontal offset between layers was also simulated, as previously reported [68]. (Figure S3). Clearly, the shoulder

peak at 5.4° is absent in the two structures. Then, two possible staggered AB packing models were calculated; however the simulated PXRD patterns did not match the experimentally observed one (Figures S4 and S5). In this case, an alternative TA-TF AA stacking model was imaginatively constructed and optimized. In this distinctive stacking structure, the Co(II)@TAPP and TFPPy vertices are alternately stacked along the z direction. In other words, a Co(II)@TAPP unit in one layer is stacked with two TFPPy units in adjacent layers along z direction. Our simulation reveals that this TA-TF AA structure is more stable than the TA-TA + TF-TF AA stacking model (48 kcal/mol lower), which can attribute to the strong interaction between positive Co(II)@TAPP and negative TFPPy. A slipped TA-TF AA structure was considered by optimizing the slipping distance Δd . The minimum (space group: P-1) was located at $\Delta d = 1.7 \text{ \AA}$ along xy direction, the energy is further lowered by 6 kcal/mol (Figure 1 insert, Figure S6). It is clear that the theoretical XRD pattern matches the experimental graph very well (Figure 1). The detailed simulation analysis was described in Section S4 in SI. Diffraction peaks at 3.6° , 4.9° , 5.4° , 7.6° , 9.7° and 11.2° were assigned to the (001), (011), (01-1), (020), (022) and (101) facets, respectively. A unit cell after refinement (space group: Triclinic P-1) with the parameters of $a = 8.59 \text{ \AA}$, $b = 23.09 \text{ \AA}$, $c = 25.89 \text{ \AA}$, $\alpha = 83.74^\circ$, $\beta = 95.01^\circ$ and $\gamma = 97.65^\circ$ was deduced (Table S2). The interlayer distance was calculated to be 3.8 \AA , which is known that it is difficult for molecules to enter the interlayers of π - π stacking architecture, while in the special structure of Co(II)@TA-TF COF, the alternately arrangement of Co(II)@TAPP and TFPPy units along z direction, as well as a 1.7 \AA slipping along xy direction gives an accessible space for small molecules (Figure 1b). As a result, it is possible to expose metal catalytic sites of Co(II)@TAPP to substrates within the adjacent stacked layers.

The cobalt content in the Co(II)@TA-TF COF was measured by inductively coupled plasma optical emission spectroscopy (ICP-OES) to be 4.2 wt%, which is less than the theoretical value of 4.6 wt%, indicating that about 91% porphyrin units were coordinated. X-ray photoelectron spectroscopy (XPS) was performed to determine the valence state of loaded cobalt (Figure S7). In comparison with cobalt acetate, both the Co $2p_{1/2}$ and Co $2p_{3/2}$ signals for Co(II)@TAPP and the Co(II)@TA-TF COF shifted to lower energy values, indicating the coordination of cobalt with porphyrin units. The binding energy values of the two signals were rather close, confirming that the Co^{2+} was not oxidized to higher valence state during the COF synthesis process.

Thermogravimetric analysis (TGA) exhibited that the Co(II)@TA-TF COF was stable up to 400°C (Figure S8). The chemical stability of the Co(II)@TA-TF COF was also investigated. The COF samples were dispersed in different solvents including THF, MeOH, water (25°C and 100°C), aqueous HCl (12 M) and NaOH (14 M) solutions for 7 days. It was found that no decomposition occurred to the Co(II)@TA-TF COF under these conditions. The samples were subjected to PXRD measurements after washing with THF and drying under vacuum at 120°C for overnight. All the samples exhibited similar PXRD patterns to its pristine Co(II)@TA-TF COF (Figure S9), indicating that the crystallinity of the COF was retained under these harsh conditions. Such a high chemical stability of the COF could be attributed to the aromatic imines with extended π - π conjugation structure that significantly improves the stability of imine linkages in acidic or basic media [50,69]. Note that, although the framework of the COF was remained, Co(II) was leached out completely after treatment in aqueous HCl (12 M) and NaOH (14 M) solutions for 7 days. Even so, our following catalytic reactions were carried out under mild conditions, the Co(II) did not leach out under the reaction conditions, as detected by CP-OES. Quasi-spherical shaped particles were observed for the Co(II)@TA-TF COF by scanning electron microscopy (SEM) (Figure S10) and transmission electron microscopy (TEM) (Figure S11), respectively. Moreover, energy dispersive X-ray spectroscopy (EDS) was also performed (Figure S12). It is clear that Co was uniformly dispersed in the COF sample.

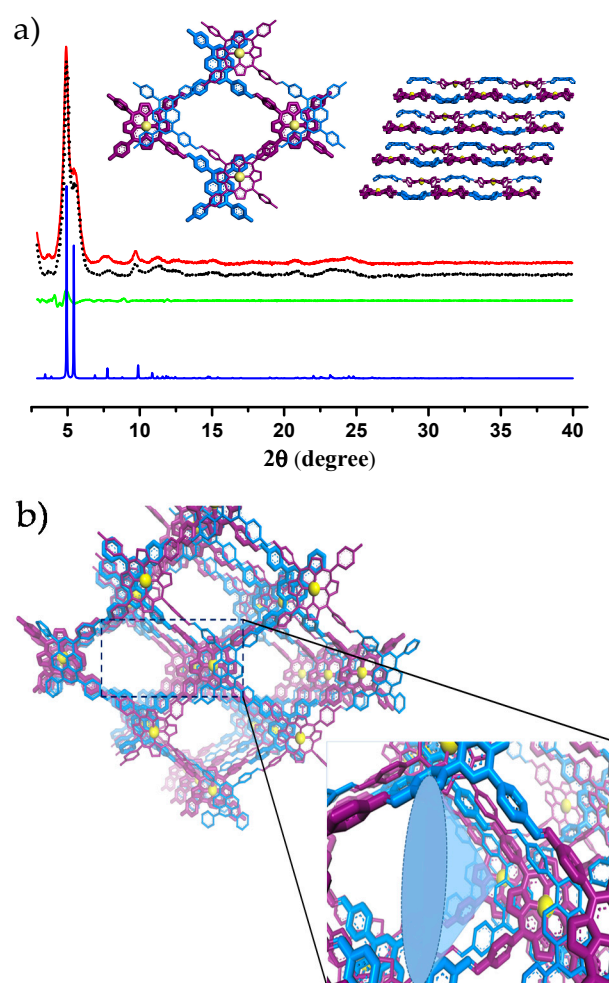


Figure 1. (a) PXRD patterns of Co(II)TA-TF COF with the observed profiles in red, refined in black, difference in green and calculated in blue. Insert: the TA-TF AA structure with a slipping distance of 1.7 Å along xy direction, and Co(II)@TAPP and TFPPy vertices are alternately stacked along the z direction. (b) Schematic representation of metal active sites of Co(II)@TAPP exposed in the pores of Co(II)@TA-TF COF.

Nitrogen sorption isotherm was measured at 77 K to further investigate the porosity of Co(II)@TA-TF COF (Figure 2a). The Brunauer–Emmett–Teller (BET) surface area of the COF was calculated to be $1076 \text{ m}^2 \text{ g}^{-1}$. The pore size distribution was evaluated by using the nonlocal density functional theory (NLDFT) method and yielded a pore size of 1.6 nm (Figure 2a, insert). These results suggest that Co(II)@TA-TF COF is a crystalline material with ordered stacking of the metalloporphyrin units. The high surface area, good stability and single type of micropores reveal that the COF could be used as catalysts for applications.

The CO_2 adsorption isotherm of the Co(II)@TA-TF COF exhibited a strong adsorption capacity of $169 \text{ mg} \cdot \text{g}^{-1}$ (i.e., 16.9 wt%) at 298 K (Figure 2b). We believe that the existence of cobalt may promote CO_2 harvesting in COF skeleton, because the incorporation of unsaturated metal sites into porous materials can dramatically increase the affinity to CO_2 [70,71]. It is worth mentioning that the CO_2 adsorption performance of the Co(II)@TA-TF COF is better than most of the COFs reported thus far (Table S3). These results pave the way towards the subsequent transformation of the adsorbed CO_2 into cyclic carbonate products catalyzed by the metalloporphyrin.

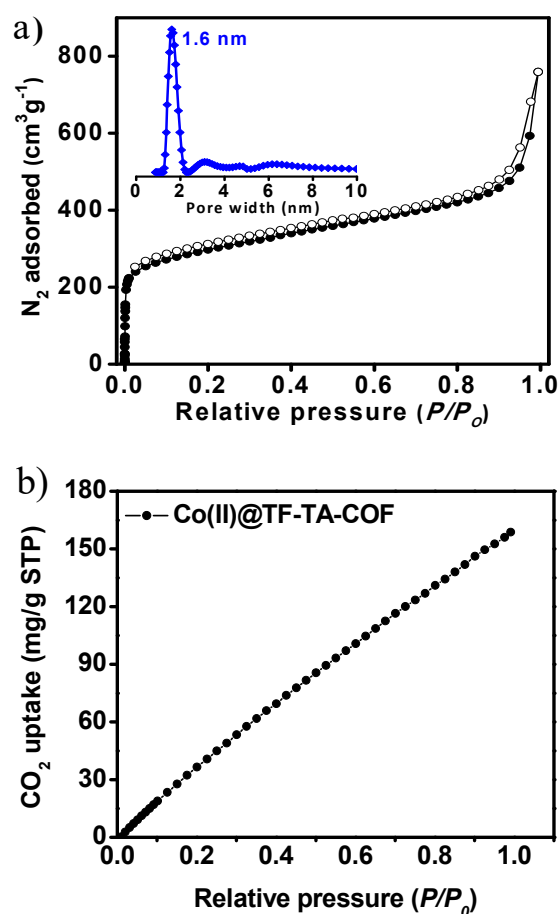


Figure 2. (a) Nitrogen sorption curves of Co(II)@TA-TF COF at 77 K (filled circles for adsorption, open circles for desorption). Insert: the pore size distribution of Co(II)@TA-TF COF and (b) CO₂ uptake ability of the Co(II)@TA-TF COF at 298 K.

2.2. Catalytic Performance of Co(II)@TA-TF COF

We employed the Co(II)@TA-TF COF for heterogeneous catalysis by taking advantage of its Lewis acid sites of metalloporphyrins, which showed excellent catalytic activity towards the cycloaddition of CO₂ and epoxides. We first investigated the effect of CO₂ pressure on the COF-catalyzed reaction under solvent-free conditions. The cycloaddition of CO₂ and epichlorohydrin was chosen as model reaction (Table 1). The yield of cyclic carbonate was higher than 90% at CO₂ pressures in the range of 0.1–0.5 MPa and temperature of 313 K, suggesting that the Co(II)@TA-TF COF exhibited excellent catalytic activity at low pressures (Table 1, entries 1–3). Temperature was found to play a crucial role in the cycloaddition of CO₂ and epichlorohydrin at 0.1 MPa. The yield increased remarkably with increasing temperature (Table 1, entries 1,4–7), which is in accordance with the results reported previously [5,24,72]. Co-catalysts were reported to have an important effect on the cycloaddition of CO₂ and epoxides [5,12,13]. In this work, co-catalyst tetrabutylammonium iodine (TBAI) exhibited a little better performance than tetrabutylammonium bromide (TBAB) and tetrabutylammonium chloride (TBAC) (Table 1, entries 1,8 and 9) because the former has a stronger nucleophilicity than the latter (i.e., Br[−] and Cl[−]) according to the principle of hard and soft acids and bases. High porosity and exposed cobalt sites of the COF may contribute to the promising catalytic performance. The catalytic performance of Co(II)@TF-TA COF was compared with previously reported COFs and MOFs catalysts (Table S4). Evidently, Co(II)@TF-TA COF has great advantages over other COFs and MOFs catalysts either in catalytic performance or in reaction conditions. Thus, the following reactions were all carried out under the conditions (0.1 MPa, 313 K, TBAI as co-catalyst).

Table 1. Influence of various experimental conditions on cycloaddition reaction ^a.

Entry	Substrate	Pressure (MPa)	Temperature (K)	Yield ^b (%)	TON	TOF (h ⁻¹)
1		0.1	313	92	460	9.6
2		0.2	313	94	470	9.8
3		0.5	313	99	495	10.3
4		0.1	298	25	125	2.6
5		0.1	303	60	300	6.3
6		0.1	323	94	470	9.8
7		0.1	343	99	495	10.3
8 ^c		0.1	313	83	415	8.6
9 ^d		0.1	313	89	445	9.3
10 ^e		0.1	313	76	380	7.9
11 ^e		0.2	313	86	430	8.9
12 ^e		0.5	313	92	460	9.6
13		0.1	313	99	495	10.3
14		0.1	298	92	460	9.6
15		0.1	313	25	125	2.6
16		0.1	313	22	110	2.3
17		0.1	313	14	70	1.5
18		0.1	313	5	25	0.52

^a Reaction conditions: Epoxide (7.5 mmol), Co(II)@TF-TA COF (32.6 mg, Co content: 0.015 mmol), co-catalyst TBAI (1.5×10^{-3} mmol), reaction time: 48 h, no additional solvent. ^b Isolated yield of the product obtained after column chromatography. ^c TBAC was used as co-catalyst. ^d TBAB was used as co-catalyst. ^e Co(II)TAPP unit was conducted as catalyst.

We also investigated the catalytic performance of the Co(II)@TAPP unit. A yield of 76% was obtained when this building unit was used as catalyst at 0.1 MPa (Table 1, entry 10). Obviously, the catalytic ability of the Co(II)@TA-TF COF is even superior to the molecular counterpart Co(II)@TAPP. We reasoned that such higher catalytic activity of the Co(II)@TA-TF COF should be mainly ascribed to the enrichment of CO₂ concentrations near the Co(II) catalytic centers in the Co(II)@TA-TF COF. To support this argument, the catalytic performance of the Co(II)@TAPP unit was tested at different CO₂ pressures. When the CO₂ pressure was increased to 0.2 MPa, a yield of 86.0% was obtained (Table 1, entry 11). With further increasing the pressure up to 0.5 MPa, the yield was enhanced to 92.0% (Table 1, entry 12). This result thus proved that the strong CO₂ adsorption capacity of the COF led to promotion in the catalytic performance. Based on the previous reports [5,12,13,70,71,73–75], it can be proposed that the cycloaddition reaction is mainly catalyzed by metalloporphyrin in conjunction with halide ions as the nucleophile [5,76]. The possible COF-based catalytic mechanism is discussed in the SI (Figure S13). To confirm the heterogeneous nature of the catalyst, an experiment was conducted in which the catalyst was removed after 20 h and the reaction was allowed to continue. As expected, the reaction did not proceed at all.

At the end of the reaction, ICP measurement of the reaction mixture filtrate showed no Co leaching, thereby establishing the truly heterogeneous nature of the catalyst.

The catalytic performance of the Co(II)@TA-TF COF in cycloaddition of CO₂ with other different epoxides under identical conditions has been examined. A higher catalytic activity was observed for cycloaddition of PO and CO₂ to form propylene carbonate with a yield of 99.0% (Table 1, entry 13). The yield of product was still high (92.0%) even when the reaction was carried out at room temperature of 298 K under 0.1 MPa (Table 1, entry 14), indicating that the Co(II)@TA-TF COF reported herein possessed excellent catalytic performance for the PO/CO₂ cycloaddition reaction at the mild reaction conditions [31,77]. Surprisingly, with increasing the molecular sizes of epoxide substrates, a remarkable decrease in the yield of cyclic carbonate was observed, as indicated by the 25% yield of 4-butyl-1,3-dioxolan-2-one (Table 1, entry 15), 21% yield of 4-(butoxymethyl)-1,3-dioxolan-2-one (Table 1, entry 16), 13% yield of 4-hexyl-1,3-dioxolan-2-one (Table 1, entry 17) and 4% yield of 4-phenyl-1,3-dioxolan-2-one (Table 1, entry 18), respectively. This result is different from the homogeneous metalloporphyrins, which generally exhibited good catalytic performance towards various epoxide substrates with less size selectivity [5,6].

The size selectivity of COFs could be ascribed to the limited space for large-sized epoxide molecules to interact with the active metalloporphyrin sites [77], as shown in Figure 1b. Due to the special structure of Co(II)@TA-TF COF, the size of epoxide substrates would be a significant factor in deciding their reaction activity and final yields. Although such a limited space is disadvantageous to the synthesis of large-sized cyclic carbonates, there was still a little amount of products obtained, which could be ascribed to the Co(II) exposed on the surface of the COFs. To verify our speculations, Raman spectra were conducted to monitor the C=C (on pyrrole moiety) stretching vibration within metalloporphyrin when the Co(II)@TA-TF COF and Co(II)@TAPP were exposed to epoxide steams for 12 h under the treatment by heating before measurement. Smaller sized epichlorohydrin and PO could interact with cobalt-porphyrin, and this caused a blue-shifting of C=C stretching vibration originally located at 1589.5 cm⁻¹ (Figure 3a). On the contrary, larger sized 1,2-epoxyoctane and styrene oxide could hardly contact Co(II) active sites, hence the C=C stretching vibration was unchanged. Since there is no steric hindrance to the interaction between the Co(II)@TAPP unit and the epoxides, blue-shifting happened to all epoxides when compared to the Co(II)@TAPP units (Figure 3b). FT-IR analysis was further carried out to confirm our speculations. The samples were treated in a same way to Raman spectra measurements. Similarly, smaller sized PO and epichlorohydrin could enter the space between adjacent COF layers and interact with cobalt-porphyrin, and this led to the disappearance of ring vibration of C-O-C epoxy group located at 1260 cm⁻¹ (Figure 4a,c). However, larger sized 1,2-epoxyoctane and styrene oxide could hardly contact Co(II) atoms, and as a result the ring vibration of epoxy group can still be observed clearly (Figure 4e,g). In the case of Co(II)@TAPP, the ring vibration peaks disappeared for all epoxides because all epoxides could interact easily with Co(II)@TAPP (Figure 4b,d,f,h).

The recyclability of the Co(II)@TA-TF COF catalyst was also evaluated. Excellent catalytic activity was maintained by this catalyst for up to five cycles (Figure S14). The crystalline structure of the COF was also found to be well preserved after each settlement (Figure S15), which highlighted the high resistance of the catalysts to the catalytic environment.

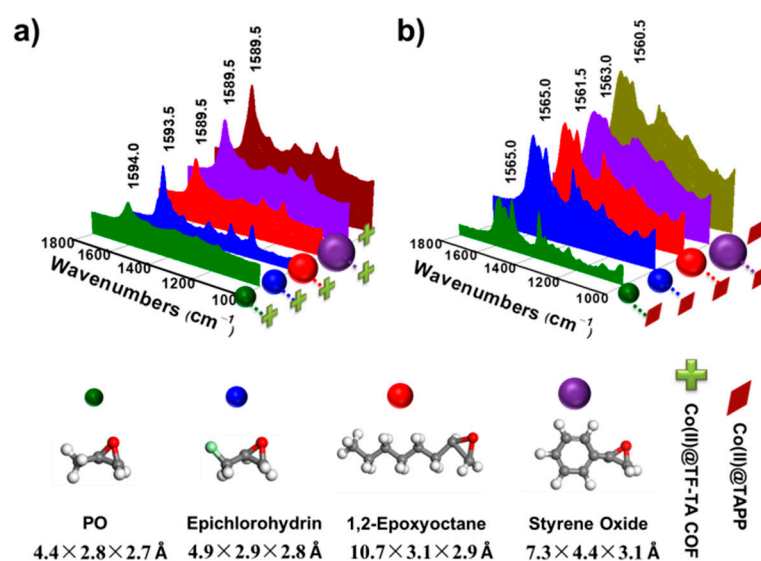


Figure 3. Raman spectra patterns of (a) Co(II)@TAPP and their epoxide complexes and (b) Co(II)@TF-TA COF and their epoxide complexes. The dimensions of epoxides are determined using MOPAC 7.

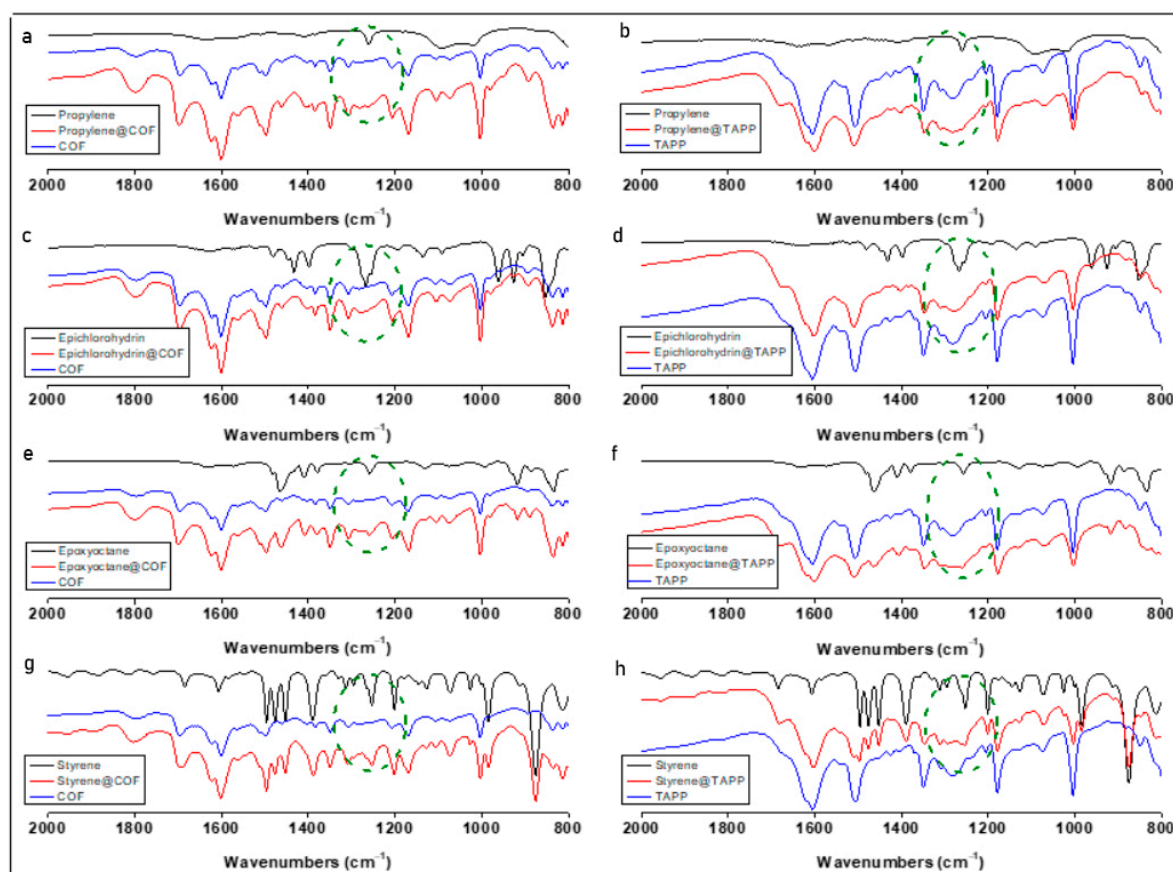


Figure 4. FT-IR spectra patterns of different sized epoxides, Co(II)@TF-TA COF, Co(II)@TAPP and their epoxide complexes. Left column: interaction information of epoxides with COF; Right column: interaction information of epoxides with TAPP. (a–d) Disappearance of ring vibration of C-O-C epoxy group located at 1260 cm^{-1} , as marked by circle (The reason is due to the interaction of small-sized epoxides with cobalt-porphyrin); (e,g) Retention of ring vibration of C-O-C epoxy group (because large-sized epoxyoctane and styrene cannot interact with cobalt-porphyrin of COF); (f,h) Disappearance of ring vibration of C-O-C epoxy group when interacting with TAPP.

3. Materials and Methods

3.1. Chemicals and Materials

Tetrakis-(triphenylphosphine) palladium (0), 4-formylbenzeneboronic acid, 1,3,6,8-tetrabromopyrene, epichlorohydrin, propylene oxide, 1,2-hexylene oxide, 1,2-epoxydecane, styrene oxide, butyl glycidyl ether, 1,3,5-mesitylene, *N,N'*-dimethylacetamide, dioxide, tetrabutylammonium iodide (TBAI) tetrabutylammonium chloride (TBAC) and tetrabutylammonium bromide (TBAB) were purchased from TCI chemicals. Other chemicals were purchased from Sinopharm Co, Shanghai, China. Carbon dioxide (99.998% purity) was purchased from the Hainan Chemical Physics of Special Gases and used as received.

3.2. Synthesis of COF Catalyst

3.2.1. Synthesis of 5,10,15,20-Tetrakis(4-aminophenyl)porphyrin (TAPP)

TAPP was synthesized according to the reported literature [78]. Typically, 4-Nitrobenzaldehyde (22.0 g, 1.45×10^{-1} mol) and acetic anhydride (24.0 mL, 2.54×10^{-1} mol) were dissolved in propionic acid (600 mL). The solution was then refluxed, to which pyrrole (10.0 mL, 1.44×10^{-1} mol) was slowly added. After refluxing for 30 min, the resulting mixture was cooled to give a precipitate which was collected by filtration, washed with H₂O and methanol, and dried under vacuum. The resulting powder was dissolved in pyridine (160 mL), which was refluxed for 1 h. After cooling, the precipitate was collected by filtration and washed with acetone to give 5,10,15,20-tetrakis(4-nitrophenyl)-21*H*,23*H*-porphine as a purple crystal in 14% yield. The product (4.13 g, 5.19×10^{-3} mol) was dissolved in hot HCl (500 mL) at 70 °C, to which was added SnCl₂·2H₂O (18.0 g, 7.97×10^{-2} mol). The resulting mixture was stirred at 70 °C for 30 min and then cooled to 0 °C. After neutralization with aqueous NH₃, the resulting gray crystalline product was collected by filtration and dissolved in acetone. Rotary evaporation of the solution followed by drying under vacuum yielded product as a purple crystal. Yield: 92%. ¹H NMR (CDCl₃, 300 MHz, ppm): δ -2.7 (s, 2H), 4.0 (s, 8H), 7.1–8.0 (m, 16H), 8.9 (s, 8H). MS (FAB, *m*-nitrobenzyl alcohol, *m/z*): Calcd for M+ 674.8; Found 675. Anal. Calcd for C₄₄H₃₄N₈: C, 78.31; H, 5.08; N, 16.61%. Found: C, 77.88; H, 5.29; N, 16.30%. UV-vis. (DMAc, λ_{max}, nm): 435, 526, 573, 665.

3.2.2. Synthesis of Cobalt(II) 5,10,15,20-Tetrakis(4-aminophenyl)porphyrin (Co(II)@TAPP)

Co(II)@TAPP was synthesized following modified procedure from reference [78]. TAPP (100 mg, 6.84×10^{-5} mol) and cobalt(II) acetate tetrahydrate (20.5 mg, 8.20×10^{-5} mol) were dissolved in DMF (20 mL), and the solution was refluxed for 5 h under argon at 130 °C. After cooling to room temperature, the resulting precipitate was collected by filtration, washed with deionized water (20 mL × 3), acetone (20 mL × 3), respectively, and dried under vacuum to yield Co(II)@TAPP as a dark purple crystal. Yield: 84%. Anal. Calcd for C₁₁₂H₁₆₀N₈O₄Co: C, 77.24; H, 9.26; N, 6.44%. Found: C, 77.89; H, 8.98; N, 6.68%. UV-vis. (DMAc, λ_{max}, nm): 440, 552, 599.

3.2.3. Synthesis of 1,3,6,8-Tetrakis(*p*-formylphenyl)pyrene (TFPPy)

TFPPy was synthesized according to modified procedure from reference [79]. A mixture of 1,3,6,8-tetrabromopyrene (1.00 g, 1.93 mmol), 4-formylphenylboronic acid (1.74 g, 11.6 mmol), palladium tetrakis(triphenylphosphine) (0.12 g, 0.10 mmol, 5.2 mol%) and potassium carbonate (2.1 g, 15 mmol) in dry dioxane (30 mL) was stirred under argon for 3 days at 85 °C. The yellow suspension reaction mixture was poured into a solution of ice-containing concentrated hydrochloric acid. The yellow solid was filtered, and washed with 2 M HCl (20 mL) three times. The product was washed with acetone (10 mL × 3), and then extracted with CHCl₃ (5 × 100 mL). The solvent was removed under reduced pressure and the resultant solid residue was recrystallized from hot CHCl₃ to afford TFPPy as a bright yellow powder (0.85 g, 72%). ¹H NMR (300 MHz, CDCl₃, d): 10.17 (s, 4H, Ar H), 8.18 (s, 4H, Ar H), 8.09 (d, *J* = 6 Hz, 8H, Ar H), 8.05 (s, 2H, Ar H), 7.86 (d, *J* = 6 Hz, 8H, Ar H).

3.2.4. Synthesis of Co(II)@TF-TA COF

In a typical procedure for the synthesis of Co(II)@TF-TA COF, a mixture of Co(II)TAPP (36.6 mg, 0.05 mmol) and TFPPy (30.9 mg, 0.05 mmol) in 1,4-dioxane/mesitylene/*N,N*-dimethylacetamide (DMAc) (7:7:5 by volume, 1.9 mL) in the presence of 0.1 mL (3 M) acetic acid in a 10 mL glass ampule vessel was degassed through three freeze-pump-thaw cycles. The vessel was evacuated to an inner pressure of ~20 Pa, flame-sealed and heated in isotherm oven at 140 °C for 3 days. The resulting precipitate was collected by centrifugation, washed thoroughly with anhydrous DMAc, tetrahydrofuran (THF), and acetone. The product was dried at 100 °C overnight under vacuum to give Co(II)@TA-TF COF (54.3 mg) in 85% yield as a brownish solid. Elemental analysis (%) calcd. for (C₈₈H₅₀N₈Co)_n: C (82.42), H (4.24), N (8.74), Co (4.6); Found: C (80.90), H (4.01), N (8.14). The Co content was measured to be 4.2 wt% by inductively coupled plasma optical emission spectroscopy (ICP-OES).

3.3. Catalyst Characterization

Elemental analysis was performed by organic elemental analyzer (vario MACRO cube, Elementar, Germany). Fourier transform infrared (FTIR) measurements were carried out on a Bruker spectrophotometer (Model TENSOR27) with powder pressed KBr pellets. Powder X-ray diffraction (PXRD) analysis was carried out on a Rigaku RINT D/Max 2500 powder diffraction system, using a Cu K α radiation ($\lambda = 1.54 \text{ \AA}$). Inductively coupled plasma optical emission spectroscopy (ICP-OES) was conducted by ICP-OES 7300 DV (PerkinElmer). The sample was firstly calcinated at 1000 °C in the air for 12 h to burn out organic moieties. The residue was dissolved by aqua regia and then diluted by water for ICP-OES testing. X-ray photoelectron spectroscopy (XPS) was recorded by ESCALAB 250Xi equipped with Al K α radiation (1486.6 eV, 200 W) on sample powder pressed pellet. Thermogravimetric analysis (TGA, STA449F3, NETZSCH, Newcastle, Germany) was performed from room temperature to above 850 °C at a heating rate of 10 °C min⁻¹ and a N₂ flow rate of 20 mL min⁻¹. The morphology of sample was observed by a transmission electron microscope (TEM, Tecnai G2 F30, FEI Company, operating at 120 kV) as well as a scanning electron microscope (SEM, Netherlands QUANTA 200 FEG) equipped with a cold field emission gun operating at 20 kV. The nitrogen physisorption experiment was conducted at 77 K on a QUADRASORB SI gas sorption system (Quantachrome Instruments), which was degassed at 120 °C under vacuum before testing. The fresh sample was activated at 100 °C for 15 h under high-vacuum conditions prior to analysis to make the pores guest-free. The specific surface areas were calculated by the Brunauer–Emmett–Teller (BET) method. The pore size distribution was evaluated by the nonlocal density function theory (NLDFT) method. Nuclear magnetic resonance (NMR) spectra were recorded by a Bruker Advance III 400 MHz NMR spectrometer (Bruker BioSpin Corporation, Fällanden, Switzerland). CO₂ adsorption measurements were conducted at 77 K. Raman spectra were performed on the Raman spectrometer (Bruker, SENTERRA) using 532 nm laser excitation.

3.4. Simulation of PXRD Patterns for Co(II)@TA-TF COF Structures

The COF models were generated using the vertex positions from the Reticular Chemistry Structure Resource. The unit cell structures (e.g., cell parameters, atomic positions, and total energies) of Co(II)@TA-TF COF were calculated using the density-functional tight-binding method including Lennard-Jones dispersion (DFTB-D), as implemented in the DFTB+ program package. Pawley refinement was carried out using Reflex, a software package for crystal determination from XRD pattern. Unit cell dimension was set to the theoretical parameters. The Pawley refinement was performed to optimize the lattice parameters iteratively until the wR_p value converges. The pseudo-Voigt profile function was used for whole profile fitting and Berrar–Baldinozzi function was used for asymmetry correction during the refinement processes. Line broadening from crystallite size and lattice strain was both considered.

3.5. General Procedures for CO₂ Cycloaddition Reaction with Epoxides

A microscale round-bottom flask was pre-dried and then charged with Co(II)@TA-TF COF (32.6 mg, containing 1.5×10^{-2} mmol of Co), co-catalyst (1.5×10^{-2} mmol) and epoxide (7.5 mmol). The flask was then equipped with a magnetic stirrer and sealed in a 50 mL Parr autoclave. The autoclave was pressurized to the appropriate pressure with CO₂ and then placed in an oil bath at desired temperature. After the reaction, a small amount of the resultant reaction mixture was removed from the autoclave for nuclear magnetic resonance (NMR) analysis to quantitatively give the conversion of epoxide. The crude product was filtered to get rid of COFs, and then purified by column chromatography. The isolated yield was calculated based on the weight of the obtained product.

4. Conclusions

In summary, a novel metalloporphyrin-containing Co(II)@TA-TF COF was designed and synthesized and this COF presented strong CO₂ adsorption capacity and high catalytic performance in cycloaddition of CO₂ and epoxides. A high yield of cyclic carbonate (i.e., 92% for chloropropene carbonate and 99% for propylene carbonate) was observed under mild conditions (at 313 K and 0.1 MPa), which is superior than the most reported COF and MOF catalytic systems. The enrichment of CO₂ concentration near the Co(II) active sites likely contributes to its enhanced catalytic performance. In the structure of Co(II)@TA-TF COF, positively charged Co(II)@TAPP and negatively charged TFPPy vertices are alternately stacked along the z direction with a slipping distance of 1.7 Å, which provides an access to small-sized substrates. Therefore, a significant substrate-size-selectivity effect was observed with Co(II)@TA-TF COF. This approach is the first example of size-selective catalysis observed in a two-dimensional COF, revealing its potential in practical application. The overall recyclability of the COF with almost unchanged reactivity for five cycles provides potential for commercially important transformation reactions.

Supplementary Materials: The following are available online at <https://www.mdpi.com/article/10.3390/catal11091133/s1>, Table S1: Elemental analysis of Co(II)@TA-TF COF, Figure S1: FTIR spectra of Co(II)@TA-TF COF, Co(II)@TAPP, TAPP and TFPPy, Figure S2: Comparison of experimentally observed PXRD pattern and calculated profile based on the true TA-TA + TF-TF AA eclipsed packing structure, Figure S3: Comparison of experimentally observed PXRD pattern and calculated profile based on the one staggered AB-stacking structure, Figure S4: Comparison of experimentally observed PXRD pattern and calculated profile based on the alternative staggered AB-stacking structure, Figure S5: Comparison of experimentally observed PXRD pattern and calculated profile based on the true TA-TF AA stacking model, Figure S6: Comparison of experimentally observed PXRD pattern and calculated profile based on the slipped TA-TF AA structure with a slight interlayer horizontal offset of 1.7 Å. This structure was described in the text, as shown by Figure 1, Table S2: Fractional atomic coordinates for unit cell of Co(II)@TA-TF COF calculated using the density-functional tight-binding method after performing the Pawley refinement, Figure S7: XPS results (Co 2p) for Co(OAc)₂, Co(II)@TAPP and Co(II)@TA-TF COF, Figure S8: TGA curve of Co(II)@TA-TF COF under N₂, Figure S9: PXRD patterns of Co(II)@TA-TF COF after treatment for one week at different conditions, Figure S10: SEM images of Co(II)@TA-TF COF, Figure S11: TEM images of Co(II)@TA-TF COF, Figure S12: EDS of Co(II)@TA-TF COF, Table S3: Comparison of CO₂ uptake ability of various COFs at 298 K, Table S4: Comparison of catalytic performance of Co(II)@TA-TF COF with previously reported COFs and MOFs, Figure S13: Scheme of possible catalytic mechanism for the reaction of epoxide and CO₂ into cyclic carbonate catalyzed by Co(II)@TA-TF COF, Figure S14: Recyclability test of the Co(II)@TA-TF COF as catalyst for the cycloaddition reaction, Figure S15: PXRD patterns of the Co(II)@TA-TF COF before and after the recycling test. Epichlorohydrin was selected as a model substrate for this reaction, and all of the other experimental parameters were identical to those presented in Table 1 in the body text.

Author Contributions: Conceptualization, Y.L., J.Z., B.W. and Y.G.; methodology, Y.L., J.Z. and K.Z.; software, H.H., B.W. and Z.L.; validation, H.X. and C.Z.; formal analysis, C.Z. and Y.W.; investigation, Y.L. and J.Z.; resources, H.X. and Y.G.; writing—original draft preparation, Y.L. and

C.Z.; writing—review and editing, B.W. and Y.G.; supervision, Y.G. All authors have read and agreed to the published version of the manuscript.

Funding: This research was funded by the Natural Science Foundation of Hainan Province (2019RC166, 2019RC110 and 2019RC250) and National Natural Science Foundation of China (21965011 and 21473196).

Institutional Review Board Statement: Not applicable.

Informed Consent Statement: Not applicable.

Data Availability Statement: Data is contained within the article and Supplementary Material.

Conflicts of Interest: The authors declare no conflict of interest.

References

1. Yang, S.H.; Sun, J.L.; Ramirez-Cuesta, A.J.; Callear, S.K.; David, W.I.F.; Anderson, D.P.; Newby, R.; Blake, A.J.; Parker, J.E.; Tang, C.C.; et al. Selectivity and direct visualisation sulfur dioxide in a decorated porous host. *Nat. Chem.* **2012**, *4*, 887–894. [[CrossRef](#)]
2. Lu, Z.Z.; Godfrey, H.; Silva, I.D.; Cheng, Y.Q.; Savage, M.; Tuna, F.; McInnes, E.; Teat, S.J.; Gagnon, K.J.; Frogley, M.D.; et al. Modulating supramolecular binding of carbon dioxide in a redox-active porous metal-organic framework. *Nat. Commun.* **2017**, *8*, 14212–14221. [[CrossRef](#)]
3. Sakakura, T.; Choi, J.C.; Yasuda, H. Transformation of carbon dioxide. *Chem. Rev.* **2007**, *107*, 2365–2387. [[CrossRef](#)] [[PubMed](#)]
4. Zhu, J.; Usov, P.M.; Xu, W.Q.; Celis-Salazar, P.J.; Lin, S.Y.; Kessinger, M.C.; Landaverde-Alvarado, C.; Cai, M.; May, A.M.; Slebodnick, C.; et al. A new class of metal-cyclam-based zirconium Metal–Organic Frameworks for CO₂ adsorption and chemical fixation. *J. Am. Chem. Soc.* **2018**, *140*, 993–1003. [[CrossRef](#)] [[PubMed](#)]
5. Maeda, C.; Taniguchi, T.; Ogawa, K.; Ema, T. Bifunctional catalysts based on m-phenylene-bridged porphyrin dimer and trimer platforms: Synthesis of cyclic carbonates from carbon dioxide and epoxides. *Angew. Chem. Int. Ed.* **2015**, *54*, 134–138. [[CrossRef](#)]
6. Darensbourg, D.J. Making plastics from carbon dioxide: Salen metal complexes as catalysts for the production of polycarbonates from epoxides and CO₂. *Chem. Rev.* **2007**, *107*, 2388–2410. [[CrossRef](#)]
7. Shen, Y.M.; Duan, W.L.; Shi, M. Chemical fixation of carbon dioxide Co-catalyzed by a combination of schiff bases or phenols and organic bases. *Eur. J. Org. Chem.* **2004**, *14*, 3080–3089. [[CrossRef](#)]
8. Wang, T.F.; Zheng, D.M.; Zhang, J.S.; Fan, B.W.; Ma, Y.; Ren, T.G.; Wang, L.; Zhang, J.L. Protic pyrazolium ionic liquids: An efficient catalyst for conversion of CO₂ in the absence of metal and solvent. *ACS Sustain. Chem. Eng.* **2018**, *6*, 2574–2582. [[CrossRef](#)]
9. Song, Q.W.; Zhou, Z.H.; He, L.N. Efficient, selective and sustainable catalysis of carbon dioxide. *Green Chem.* **2017**, *19*, 3707–3728. [[CrossRef](#)]
10. Li, C.; Liu, F.; Zhao, T.X.; Gu, J.R.; Chen, P.; Chen, T. Highly efficient CO₂ fixation into cyclic carbonate by hydroxyl-functionalized protic ionic liquids at atmospheric pressure. *Mol. Catal.* **2021**, *511*, 111756. [[CrossRef](#)]
11. Aomchad, V.; Gobbo, S.D.; Yingcharoen, P.; Poater, A.; D’Elia, V. Exploring the potential of group III salen complexes for the conversion of CO₂ under ambient conditions. *Catal. Today* **2021**, *375*, 324–334. [[CrossRef](#)]
12. Zhou, F.; Xie, S.L.; Gao, X.T.; Zhang, R.; Wang, C.H.; Yin, G.Q.; Zhou, J. Activation of (salen)CoI complex by phosphorane for carbon dioxide transformation at ambient temperature and pressure. *Green Chem.* **2017**, *19*, 3908–3915. [[CrossRef](#)]
13. Ema, T.; Miyazaki, Y.; Shimonishi, J.; Maeda, C.; Hasegawa, J. Bifunctional porphyrin catalysts for the synthesis of cyclic carbonates from epoxides and CO₂: Structural optimization and mechanistic study. *J. Am. Chem. Soc.* **2014**, *136*, 15270–15279. [[CrossRef](#)] [[PubMed](#)]
14. Maeda, C.; Shimonishi, J.; Miyazaki, R.; Hasegawa, J.; Ema, T. Highly active and robust metalloporphyrin catalysts for the synthesis of cyclic carbonates from a broad range of epoxides and carbon dioxide. *Chem. Eur. J.* **2016**, *22*, 6556–6563. [[CrossRef](#)]
15. Al-Rawi, U.A.; Sher, F.; Hazafa, A.; Rasheed, T.; Al-Shara, N.K.; Lima, E.C.; Shanshool, J. Catalytic Activity of Pt Loaded Zeolites for Hydroisomerization of n-Hexane Using Supercritical CO₂. *Ind. Eng. Chem. Res.* **2020**, *59*, 22092–22106. [[CrossRef](#)]
16. Sher, F.; Yaqoob, A.; Saeed, F.; Zhang, S.F.; Jahan, Z.; Klemeš, J.J. Torrefied biomass fuels as a renewable alternative to coal in co-firing for power generation. *Energy* **2020**, *209*, 118444. [[CrossRef](#)]
17. Al-Juboori, O.; Sher, F.; Khalid, U.; Niazi, M.; Chen, G.Z. Electrochemical Production of Sustainable Hydrocarbon Fuels from CO₂ Co-electrolysis in Eutectic Molten Melts. *ACS Sustain. Chem. Eng.* **2020**, *8*, 12877–12890. [[CrossRef](#)]
18. Rasheed, T.; Hassan, A.A.; Kausar, F.; Sher, F.; Bilal, M.; Iqbal, H. Carbon nanotubes assisted analytical detection-Sensing/delivery cues for environmental and biomedical monitoring. *TrAC-Trend Anal. Chem.* **2020**, *132*, 116066. [[CrossRef](#)]
19. Bhat, S.A.; Bashir, O.; Bilal, M.; Ishaq, A.; Dar, M.U.D.; Kumar, R.; Bhat, R.A.; Sher, F. Impact of COVID-related lockdowns on environmental and climate change scenarios. *Environ. Res.* **2021**, *195*, 110839. [[CrossRef](#)]
20. Zhang, Y.; Ran, Z.Z.; Jin, B.S.; Zhang, Y.W.; Zhou, C.L.; Sher, F. Simulation of Particle Mixing and Separation in Multi-Component Fluidized Bed Using Eulerian-Eulerian Method: A Review. *Int. J. Chem. React. Eng.* **2019**, *17*. [[CrossRef](#)]
21. Ahmed, M.; Sakthivel, A. Preparation of cyclic carbonate via cycloaddition of CO₂ on epoxide using amine-functionalized SAPO-34 as catalyst. *J. CO₂ Util.* **2017**, *22*, 392–399. [[CrossRef](#)]

22. Bhin, K.M.; Tharun, J.; Roshan, K.R.; Kim, D.W.; Chung, Y.; Park, D.W. Catalytic performance of zeolitic imidazolate framework ZIF-95 for the solventless synthesis of cyclic carbonates from CO₂ and epoxides. *J. CO₂ Util.* **2017**, *17*, 112–118. [[CrossRef](#)]
23. Yamazaki, K.; Moteki, T.; Ogura, M. Carbonate synthesis from carbon dioxide and cyclic ethers over methylated nitrogensubstituted mesoporous silica. *Mol. Catal.* **2018**, *454*, 38–43. [[CrossRef](#)]
24. Zhang, S.; Liu, X.; Li, M.; Wei, Y.; Zhang, G.; Han, J.; Zhu, X.; Ge, Q.; Wang, H. Metal-free amino-incorporated organosilica nanotubes for cooperative catalysis in the cycloaddition of CO₂ to epoxides. *Catal. Today* **2019**, *324*, 59–65. [[CrossRef](#)]
25. Xie, Y.; Zhang, Z.F.; Jiang, T.; He, J.L.; Han, B.X.; Wu, T.B.; Ding, K.L. CO₂ cycloaddition reactions catalyzed by an ionic liquid grafted onto a highly cross-linked polymer matrix. *Angew. Chem. Int. Ed.* **2007**, *46*, 7255–7258. [[CrossRef](#)] [[PubMed](#)]
26. Zhong, H.; Su, Y.; Chen, X.; Li, X.; Wang, R. Imidazolium- and triazine-based porous organic polymers for heterogeneous catalytic conversion of CO₂ into cyclic carbonates. *ChemSusChem* **2017**, *10*, 4855–4863. [[CrossRef](#)]
27. Verma, S.; Kumar, G.; Ansari, A.; Kureshy, R.I.; Khan, N.H. A nitrogen rich polymer as an organo-catalyst for cycloaddition of CO₂ to epoxides and its application for the synthesis of polyurethane. *Sustain. Energy Fuels* **2017**, *1*, 1620–1629. [[CrossRef](#)]
28. Ma, D.; Liu, K.; Li, J.; Shi, Z. Bifunctional metal-free porous organic framework heterogeneous catalyst for efficient CO₂ conversion under mild and cocatalyst-free conditions. *ACS Sustain. Chem. Eng.* **2018**, *6*, 15050–15055. [[CrossRef](#)]
29. Ravi, S.; Puthiaraj, P.; Ahn, W.S. Hydroxylamine-anchored covalent aromatic polymer for CO₂ adsorption and fixation into cyclic carbonates. *ACS Sustain. Chem. Eng.* **2018**, *6*, 9324–9332. [[CrossRef](#)]
30. Ma, R.; He, L.N.; Zhou, Y.B. Efficient and recyclable tetraoxo-coordinated zinc catalyst for the cycloaddition of epoxides with carbon dioxide at atmospheric pressure. *Green Chem.* **2016**, *18*, 226–231. [[CrossRef](#)]
31. Marciniak, A.A.; Lamb, K.J.; Ozorio, L.P.; Mota, C.J.A.; North, M. Heterogeneous catalysts for cyclic carbonate synthesis from carbon dioxide and epoxides. *Curr. Opin. Green Sustain. Chem.* **2020**, *26*, 100365–100394. [[CrossRef](#)]
32. Xie, Y.; Wang, T.T.; Liu, X.H.; Zou, K.; Deng, W.Q. Capture and conversion of CO₂ at ambient conditions by a conjugated microporous polymer. *Nat. Commun.* **2013**, *4*, 1960–1966. [[CrossRef](#)]
33. Beyzavi, M.H.; Klet, R.C.; Tussupbayev, S.; Borycz, J.; Vermeulen, N.A.; Cramer, C.J.; Stoddart, J.F.; Hupp, J.T.; Farha, O.K. A hafnium-based metal-organic framework as an efficient and multifunctional catalyst for facile CO₂ fixation and regioselective and enantioselective epoxide activation. *J. Am. Chem. Soc.* **2014**, *136*, 15861–15864. [[CrossRef](#)] [[PubMed](#)]
34. Furukawa, Y.H.; Yaghi, O.M. Storage of hydrogen, methane, and carbon dioxide in highly porous covalent organic frameworks for clean energy applications. *J. Am. Chem. Soc.* **2009**, *131*, 8875–8883. [[CrossRef](#)]
35. Duan, K.; Wang, J.; Zhang, Y.T.; Liu, J.D. Covalent organic frameworks (COFs) functionalized mixed matrix membrane for effective CO₂/N₂ separation. *J. Membr. Sci.* **2019**, *572*, 588–595. [[CrossRef](#)]
36. Giri, A.; Hopkins, P.E. Heat Transfer Mechanisms and Tunable Thermal Conductivity Anisotropy in Two-Dimensional Covalent Organic Frameworks with Adsorbed Gases. *Nano Lett.* **2021**, *21*, 6188–6193. [[CrossRef](#)]
37. Ma, H.P.; Ren, H.; Meng, S.; Yan, Z.J.; Sun, F.X.; Zhu, G.S. A 3D microporous covalent organic framework with exceedingly high C₃H₈/CH₄ and C₂ hydrocarbon/CH₄ selectivity. *Chem. Commun.* **2013**, *49*, 9773–9775. [[CrossRef](#)]
38. Oh, H.; Kalidindi, S.B.; Um, Y.; Bureekaew, S.; Schmid, R.; Fischer, R.A.; Hirscher, M. A cryogenically flexible covalent organic framework for efficient hydrogen isotope separation by quantum sieving. *Angew. Chem. Int. Ed.* **2013**, *52*, 13219–13222. [[CrossRef](#)] [[PubMed](#)]
39. Zhai, L.P.; Huang, N.; Xu, H.; Chen, Q.H.; Jiang, D.L. A backbone design principle for covalent organic frameworks: The impact of weakly interacting units on CO₂ adsorption. *Chem. Commun.* **2017**, *53*, 4242–4245. [[CrossRef](#)] [[PubMed](#)]
40. Stegbauer, L.; Hahn, M.W.; Jentys, A.; Savasci, G.; Ochsenfeld, C.; Lercher, J.A.; Lotsch, B.V. Tunable water and CO₂ sorption properties in isostructural azine-based covalent organic frameworks through polarity engineering. *Chem. Mater.* **2015**, *27*, 7874–7881. [[CrossRef](#)]
41. Baldwin, L.A.; Crowe, J.W.; Pyles, D.A.; McGrier, P.L. Metalation of a mesoporous three-dimensional covalent organic framework. *J. Am. Chem. Soc.* **2016**, *138*, 15134–15137. [[CrossRef](#)] [[PubMed](#)]
42. Huang, N.; Wang, P.; Addicoat, M.A.; Heine, T.; Jiang, D.L. Ionic covalent organic frameworks: Design of a charged interface aligned on 1D channel walls and its unusual electrostatic functions. *Angew. Chem. Int. Ed.* **2017**, *56*, 4982–4986. [[CrossRef](#)] [[PubMed](#)]
43. Dey, K.; Pal, M.; Rout, K.C.; Kunjattu, H.S.; Das, A.; Mukherjee, R.; Kharul, U.K.; Banerjee, R. Selective molecular separation by interfacially crystallized covalent organic framework thin films. *J. Am. Chem. Soc.* **2017**, *139*, 13083–13091. [[CrossRef](#)]
44. Fang, Q.R.; Gu, S.; Zheng, J.; Zhuang, Z.; Qiu, S.L.; Yan, Y.S. Cheminform abstract: 3D microporous base-functionalized covalent organic frameworks for size-selective catalysis. *Angew. Chem. Int. Ed.* **2014**, *53*, 2878–2882. [[CrossRef](#)] [[PubMed](#)]
45. Pachfule, P.; Kandambeth, S.; Banerjee, R. Highly stable covalent organic framework-au nanoparticles hybrids for enhanced activity for nitrophenol reduction. *Chem Commun.* **2014**, *50*, 3169–3172. [[CrossRef](#)]
46. Xu, H.; Gao, J.; Jiang, D. Stable, crystalline, porous, covalent organic frameworks as a platform for chiral organocatalysts. *Nat. Chem.* **2015**, *7*, 905–912. [[CrossRef](#)]
47. Xu, H.S.; Ding, S.Y.; An, W.K.; Wu, H.; Wang, W. Constructing crystalline covalent organic frameworks from chiral building blocks. *J. Am. Chem. Soc.* **2016**, *138*, 11489–11492. [[CrossRef](#)]
48. Wang, K.; Yang, L.M.; Wang, X.; Guo, L.; Guang, C.; Zhang, C.; Jin, S.; Tan, B.; Cooper, A. Covalent triazine frameworks via a low-temperature polycondensation approach. *Angew. Chem. Int. Ed.* **2017**, *56*, 14149–14153. [[CrossRef](#)]

49. Li, L.H.; Feng, X.L.; Cui, X.H.; Ma, Y.X.; Ding, S.Y.; Wang, W. Salen-based covalent organic framework. *J. Am. Chem. Soc.* **2017**, *139*, 6042–6045. [[CrossRef](#)]
50. Sun, Q.; Aguila, B.; Perman, J.; Nguyen, N.; Ma, S.Q. Flexibility matters: Cooperative active sites in covalent organic framework and threaded ionic polymer. *J. Am. Chem. Soc.* **2016**, *138*, 15790–15796. [[CrossRef](#)]
51. Wang, X.R.; Han, X.; Zhang, J.; Wu, X.W.; Liu, Y.; Cui, Y. Multivariate chiral covalent organic frameworks with controlled crystallinity and stability for asymmetric catalysis. *J. Am. Chem. Soc.* **2017**, *139*, 8277–8285.
52. Han, X.; Xia, Q.C.; Huang, J.J.; Liu, Y.; Tan, C.X.; Cui, Y. Chiral covalent organic frameworks with high chemical stability for heterogeneous asymmetric catalysis. *J. Am. Chem. Soc.* **2017**, *139*, 8693–8697. [[CrossRef](#)]
53. Sick, T.; Hufnagel, A.G.; Kampmann, J.; Kondofersky, L.; Calik, M.; Rotter, J.M.; Evans, A.; Döblinger, M.; Herbert, S.; Peters, K.; et al. Oriented films of conjugated 2D covalent organic frameworks as photocathodes for water splitting. *J. Am. Chem. Soc.* **2018**, *140*, 2085–2092. [[CrossRef](#)] [[PubMed](#)]
54. Calik, M.; Auras, F.; Salonen, L.M.; Bader, K.; Grill, I.; Handloser, M.; Medina, D.D.; Dogru, M.; Löbermann, F.; Trauner, D.; et al. Extraction of photogenerated electrons and holes from a covalent organic framework integrated heterojunction. *J. Am. Chem. Soc.* **2014**, *136*, 17802–17807. [[CrossRef](#)] [[PubMed](#)]
55. Keller, N.; Bessinger, D.; Reuter, S.; Calik, M.; Ascherl, L.; Hanusch, F.C.; Auras, F.; Bein, T. Oligothiophene-bridged conjugated covalent organic frameworks. *J. Am. Chem. Soc.* **2017**, *139*, 8194–8199. [[CrossRef](#)]
56. Segura, J.L.; Mancheño, M.J.; Zamora, F. Covalent organic frameworks based on schiff-base chemistry: Synthesis, properties and potential applications. *Chem. Soc. Rev.* **2016**, *45*, 5635–5671. [[CrossRef](#)]
57. Diercks, C.S.; Yaghi, O.M. The atom, the molecule, and the covalent organic framework. *Science* **2017**, *355*, 1585–1593. [[CrossRef](#)] [[PubMed](#)]
58. Huang, N.; Wang, P.; Jiang, D.L. Covalent organic frameworks: A materials platform for structural and functional designs. *Nat. Rev. Mater.* **2016**, *1*, 16068–16087. [[CrossRef](#)]
59. Wei, H.; Chai, S.Z.; Hu, N.T.; Yang, Z.; Wei, L.M.; Wang, L. The microwave-assisted solvothermal synthesis of a crystalline two-dimensional covalent organic framework with high CO₂ capacity. *Chem. Commun.* **2015**, *51*, 12178–12181. [[CrossRef](#)]
60. Huang, N.; Chen, X.; Krishna, R.; Jiang, D.L. Two-dimensional covalent organic frameworks for carbon dioxide capture through channel-wall functionalization. *Angew. Chem. Int. Ed.* **2015**, *54*, 2986–2990. [[CrossRef](#)] [[PubMed](#)]
61. Huang, N.; Krishna, R.; Jiang, D. Tailor-made pore surface engineering in covalent organic frameworks: Systematic functionalization for performance screening. *J. Am. Chem. Soc.* **2015**, *137*, 7079–7082. [[CrossRef](#)]
62. Yang, F.; Li, Y.; Zhang, T.; Zhao, Z.; Xing, G.; Chen, L. Docking site modulation of isostructural covalent organic frameworks for CO₂ fixation. *Chem. Eur. J.* **2020**, *26*, 4510–4514. [[CrossRef](#)]
63. Zhi, Y.; Shao, P.; Feng, X.; Xia, H.; Zhang, Y.; Shi, Z.; Mu, Y.; Liu, X. Covalent organic frameworks: Efficient, metal-free, heterogeneous organocatalysts for chemical fixation of CO₂ under mild conditions. *J. Mater. Chem. A* **2018**, *6*, 374–382. [[CrossRef](#)]
64. Liu, J.; Zhao, G.; Cheung, O.; Jia, L.; Sun, Z.; Zhang, S. Highly porous metalloporphyrin covalent ionic frameworks with well-defined cooperative functional groups as excellent catalysts for CO₂ cycloaddition. *Chem. Eur. J.* **2019**, *25*, 9052–9059. [[CrossRef](#)] [[PubMed](#)]
65. Xu, K.; Dai, Y.; Ye, B.; Wang, H. Two dimensional covalent organic framework materials for chemical fixation of carbon dioxide: Excellent repeatability and high selectivity. *Dalton Trans.* **2017**, *46*, 10780–10785. [[CrossRef](#)]
66. Zhang, Y.; Hu, H.; Ju, J.; Yan, Q.; Arumugam, V.; Jing, X.; Cai, H.; Gao, Y. Ionization of a covalent organic framework for catalyzing the cycloaddition reaction between epoxides and carbon dioxide. *Chin. J. Catal.* **2020**, *41*, 485–493. [[CrossRef](#)]
67. Ding, L.; Yao, B.; Wu, W.; Yu, Z.; Wang, X.; Kan, J.; Dong, Y. Metalloporphyrin and ionic liquid-functionalized covalent organic frameworks for catalytic CO₂ cycloaddition via visible-light-induced photothermal conversion. *Inorg. Chem.* **2021**, *60*, 12591–12601. [[CrossRef](#)]
68. Du, Y.R.; Ding, G.R.; Wang, Y.F.; Xu, B.H.; Zhang, S.J. Construction of a PPIL@COF core-shell composite with enhanced catalytic activity for CO₂ conversion. *Green Chem.* **2021**, *23*, 2411–2419. [[CrossRef](#)]
69. Sengupta, M.; Bag, A.; Ghosh, S.; Mondal, P.; Bordoloi, A.; Islam, S.M. Cu_xO_y@COF: An efficient heterogeneous catalyst system for CO₂ cycloadditions under ambient conditions. *J. CO₂ Util.* **2019**, *34*, 533–542. [[CrossRef](#)]
70. Spitler, E.L.; Koo, B.T.; Novotney, J.L.; Colson, J.W.; Uribe-Romo, F.J.; Gutierrez, G.D.; Clancy, P.; Dichtel, W.R. A 2D covalent organic framework with 4.7-nm pores and insight into its interlayer stacking. *J. Am. Chem. Soc.* **2011**, *133*, 19416–19421. [[CrossRef](#)] [[PubMed](#)]
71. Matesic, L.; Locke, J.M.; Vine, K.L.; Ranson, M.; Bremner, J.B.; Skropeta, D. Synthesis and hydrolytic evaluation of acid-labile imine-linked cytotoxic isatin model systems. *Bioorg. Med. Chem.* **2011**, *19*, 1771–1778. [[CrossRef](#)] [[PubMed](#)]
72. Müller, I.A.; Kratz, F.; Jung, M.; Warnecke, A. Schiff bases derived from p-aminobenzyl alcohol as trigger groups for pH-dependent prodrug activation. *Tetrahedron Lett.* **2010**, *51*, 4371–4374. [[CrossRef](#)]
73. Feng, D.; Chung, W.C.; Wei, Z.; Gu, Z.Y.; Jiang, H.L.; Chen, Y.P.; Darensbourg, D.J.; Zhou, H.C. Construction of ultrastable porphyrin Zr metal-organic frameworks through linker elimination. *J. Am. Chem. Soc.* **2013**, *135*, 17105–17110. [[CrossRef](#)]
74. Gao, W.Y.; Chen, Y.; Niu, Y.; Williams, K.; Cash, L.; Perez, P.J.; Wojtas, L.; Cai, J.; Chen, Y.S.; Ma, S. Crystal engineering of an *nbo* topology metal-organic framework for chemical fixation of CO₂ under ambient conditions. *Angew. Chem. Int. Ed.* **2014**, *53*, 2615–2619. [[CrossRef](#)]

75. Chen, J.; Zhong, M.M.; Tao, L.; Liu, L.N.; Jayakumar, S.; Li, C.Z.; Li, H.; Yang, Q.H. The cooperation of porphyrin-based porous polymer and thermal-responsive ionic liquid for efficient CO₂ cycloaddition reaction. *Green Chem.* **2018**, *20*, 903–911. [[CrossRef](#)]
76. Song, J.L.; Zhang, Z.F.; Hu, S.Q.; Wu, T.B.; Jiang, T.; Han, B.X. MOF-5/n-Bu₄NBr: An efficient catalyst system for the synthesis of cyclic carbonates from epoxides and CO₂ under mild conditions. *Green Chem.* **2009**, *11*, 1031–1036. [[CrossRef](#)]
77. Wu, G.P.; Ren, W.M.; Luo, Y.; Li, B.; Zhang, W.Z.; Lu, X.B. Enhanced asymmetric induction for the copolymerization of CO₂ and cyclohexene oxide with unsymmetric enantiopure salenCo(III) complexes: Synthesis of crystalline CO₂-based polycarbonate. *J. Am. Chem. Soc.* **2012**, *134*, 5682–5688. [[CrossRef](#)]
78. Li, P.Z.; Wang, X.J.; Liu, J.; Lim, S.; Zou, R.Q.; Zhao, Y.L. A triazole-containing metal-organic framework as a highly effective and substrate size-dependent catalyst for CO₂ conversion. *J. Am. Chem. Soc.* **2016**, *138*, 2142–2145. [[CrossRef](#)] [[PubMed](#)]
79. Ju, H.Y.; Manju, M.D.; Kim, K.H.; Park, S.W.; Park, D.W. Catalytic performance of quaternary ammonium salts in the reaction of butyl glycidyl ether and carbon dioxide. *J. Ind. Eng. Chem.* **2008**, *14*, 157–160. [[CrossRef](#)]